Scaling properties of discontinuous maps

J. A. Méndez-Bermúdez[1] and R. Aguilar-Sánchez[2]
[1]*Instituto de Física, Benemérita Universidad Autónoma de Puebla, Apartado Postal J-48, Puebla 72570, Mexico*
[2]*Facultad de Ciencias Químicas, Benemérita Universidad Autónoma de Puebla, Puebla 72570, Mexico*
(Received 29 January 2012; revised manuscript received 1 May 2012; published 25 May 2012)

We study the scaling properties of discontinuous maps by analyzing the average value of the squared action variable I^2. We focus our study on two dynamical regimes separated by the critical value K_c of the control parameter K: the slow diffusion ($K < K_c$) and the quasilinear diffusion ($K > K_c$) regimes. We found that the scaling of I^2 for discontinuous maps when $K \ll K_c$ and $K \gg K_c$ obeys the same scaling laws, in the appropriate limits, as Chirikov's standard map in the regimes of weak and strong nonlinearity, respectively. However, due to the absence of Kolmogorov-Arnold-Moser tori, we observed in both regimes that $I^2 \propto nK^\beta$ for $n \gg 1$ (n being the nth iteration of the map) with $\beta \approx 5/2$ when $K \ll K_c$ and $\beta \approx 2$ for $K \gg K_c$.

DOI: 10.1103/PhysRevE.85.056212 PACS number(s): 05.45.Pq

I. INTRODUCTION AND MODEL

Chirikov's standard map (CSM), introduced in Ref. [1], is an area preserving two-dimensional (2D) map for action and angle variables (I,θ):

$$\begin{aligned} I_{n+1} &= I_n + Kf(\theta_n), \\ \theta_{n+1} &= \theta_n + I_{n+1}, \quad \mathrm{mod} - 2\pi, \end{aligned} \tag{1}$$

where $f(\theta_n) = \sin(\theta_n)$ [due to this choice of $f(\theta)$, CSM is identified as a *continuous* map]. CSM describes the situation when nonlinear resonances are equidistant in phase space which corresponds to a local description of dynamical chaos [2]. Due to this property various dynamical systems and maps can be locally reduced to map (1). Thus, CSM describes the universal and generic behavior of nearly integrable Hamiltonian systems with two degrees of freedom having a divided phase space composed of stochastic motion bounded by invariant tori [also known as the Kolmogorov-Arnold-Moser (KAM) scenario] [2].

CSM develops two dynamical regimes separated by the critical parameter K_c [1–7]. When $K < K_c$, the regime of weak nonlinearity, the motion is mainly regular with regions of stochasticity and I is bounded by KAM surfaces. See, for example, Fig. 1(a) where we present the Poincaré surface of section for CSM with $K = 0.01$. Here, the value of K is so small that the Poincaré surface of section is equivalent to the phase portrait of a one-dimensional pendulum. At $K = K_c$, the last KAM curve is destroyed and the transition to global stochasticity takes place. Then, for $K > K_c$, the regime of strong nonlinearity, I becomes unbounded and increases diffusively. See, for example, the Poincaré map of Fig. 1(b) where a single trajectory has been iterated 3×10^4 times.

Even though CSM describes the universal behavior of area-preserving continuous maps, another class of Hamiltonian dynamical systems is represented by the *discontinuous* map [8]:

$$\begin{aligned} I_{n+1} &= I_n + Kf(\theta_n), \\ \theta_{n+1} &= \theta_n + TI_{n+1}, \quad \mathrm{mod} - 2\pi, \end{aligned} \tag{2}$$

where $f(\theta_n) = \sin(\theta_n)\mathrm{sgn}[\cos(\theta_n)]$. Examples of physical systems described by discontinuous maps are 2D billiard models, like the stadium billiard [9,10], and polygonal billiards [11,12]. The origin of the discontinuity in map (2) is the sudden translations of the action under the system dynamics.

As well as CSM, map (2) is known to have two different dynamical regimes; however both are diffusive, delimited by the critical value $K_c = 1/T$ [8]. The regimes $K < K_c$ and $K > K_c$ are known as slow diffusion and quasilinear diffusion regimes, respectively. As an example of the dynamics of map (2), in Fig. 2 we show typical Poincaré surface of sections in both regimes (for comparison purposes we have used the same values of K as in Fig. 1 for CSM). On the one hand, as can be observed by contrasting Figs. 1(a) and 2(a), the main difference between CSM and map (2) is that for $K < K_c$ the latter does not show regular behavior. In fact, due to the discontinuities of $f(\theta)$ in map (2), the KAM theorem is not satisfied and map (2) does not develop the KAM scenario. Since for any $K \neq 0$ the dynamics of map (2) is diffusive, a single trajectory can explore the entire phase space. However, in the slow diffusion regime the dynamics is far from being stochastic due to the sticking of trajectories along cantori (fragments of KAM invariant tori) [see Fig. 2(a)]. On the other hand, for $K > K_c$ map (2) shows diffusion similar to that of CSM [compare Figs. 1(b) and 2(b)]. We want to add that independent of the value of $K \neq 0$, map (2) has five period-one fixed points at $I = 0$ and $\theta = [0,\pi/2,\pi,3\pi/2,2\pi]$.

In particular, in Ref. [13] a scaling analysis of CSM was performed by studying the average value of I^2 as a function of K and the nth iteration of the map. There, the following scaling law was reported:

$$I^2 \propto n^\alpha K^\beta, \tag{3}$$

where $\alpha \approx 2$ for $K \ll K_c$ and small n while $\alpha \approx 1$ for $K \gg K_c$ and large n, with $\beta \approx 2$ in both cases. The scaling (3) has also been validated for several dynamical systems represented by the standard map, such as the Fermi-Ulam model [14–18], time-dependent potential wells [19], and waveguide billiards [18,20] among others [21,22].

Since map (2) has the same structure as CSM, a systematic investigation of the scaling properties of I^2 for discontinuous maps is undertaken in this paper. For this purpose, here we study the properties of the map of Eq. (2) by analyzing the scaling of the average value of the squared action variable I^2 as a function of n, K, and I_0. We choose the scaling approach

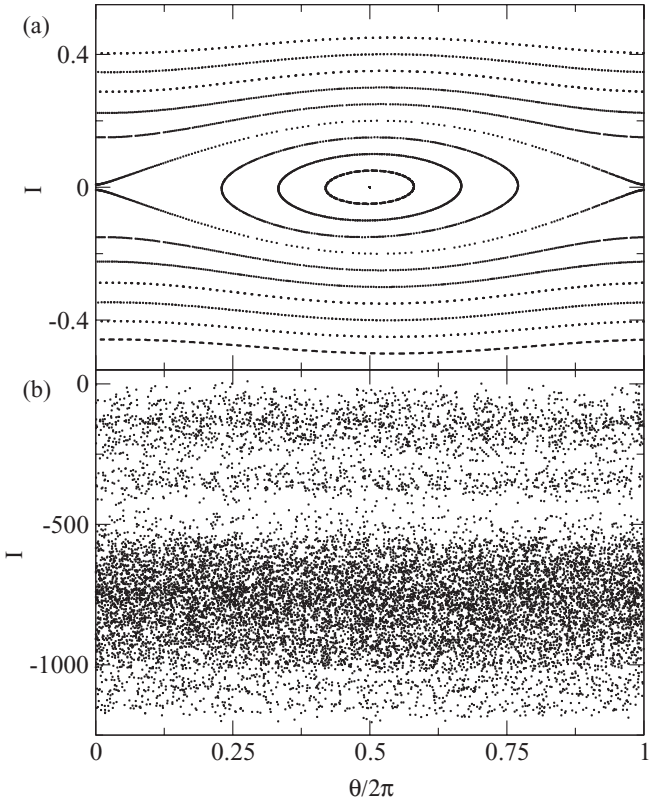

FIG. 1. Poincaré surface of section for CSM, Eq. (1), with (a) $K = 0.01$ and (b) $K = 10$. In (a) 20 initial conditions with $\theta_0 = \pi$ and $I_0 = [-0.5, 0.5)$ were iterated 10^3 times. In (b) a single initial condition with $\theta_0 = 3$ and $I_0 = 0.01$ was iterated 3×10^4 times.

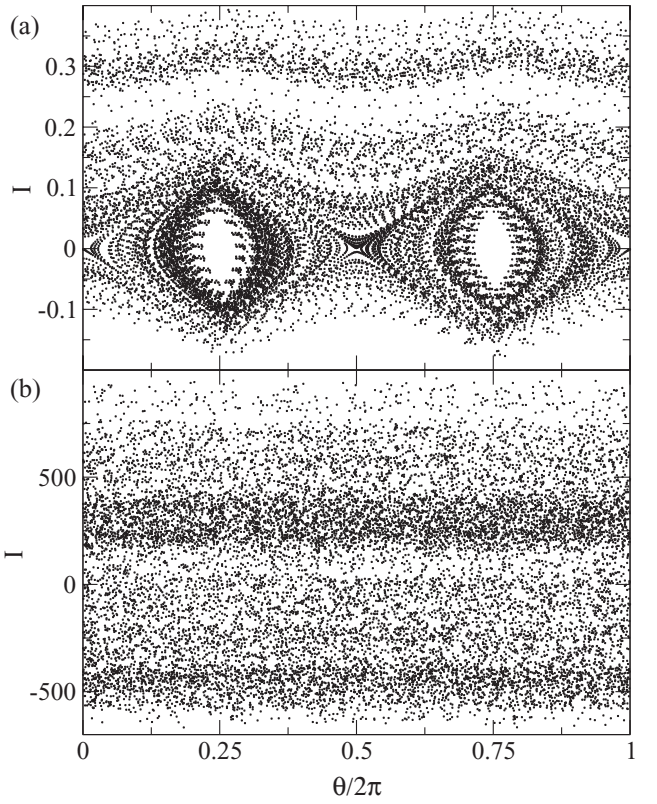

FIG. 2. Poincaré surface of section for the discontinuous map of Eq. (2) with (a) $K = 0.01$ and (b) $K = 10$. $T = 1$. A single initial condition with $\theta_0 = 3$ and $I_0 = 0.01$ was iterated 3×10^4 times.

to I^2 reported in Ref. [13] because of the similarity of maps (1) and (2). Moreover, since map (2) shows diffusion in both dynamical regimes ($K < K_c$ and $K > K_c$), we expect the scaling (3) to be valid for discontinuous maps when diffusion is present with scaling exponents α and β to be determined.

II. RESULTS

We compute I^2 for map (2) following two steps [13]: First we calculate the average squared action over the orbit associated with the initial condition j as

$$\langle I_{n,j}^2 \rangle = \frac{1}{n+1} \sum_{i=0}^{n} I_{i,j}^2,$$

where i refers to the ith iteration of the map. Then, the average value of I^2 is defined as the average over M independent realizations of the map (by randomly choosing values of θ_0):

$$I^2(n, K, I_0) = \frac{1}{M} \sum_{j=1}^{M} \langle I_{n,j}^2 \rangle. \tag{4}$$

In the following, without lost of generality, we set $T = 1$.

A. Slow diffusion regime

In Fig. 3(a) we present I^2 as a function of n in the slow diffusion regime ($K \ll 1$) for several combinations of K and I_0. In fact, I^2 is always an increasing function of n; however its growth is marginal in some iteration intervals producing plateaus in the curves I^2 vs n.

For $I_0 \ll K$, see full symbols in Fig. 3(a), I^2 grows up to a crossover iteration number $n_{\rm cr}^{(1)}$. When $n_{\rm cr}^{(1)} < n < n_{\rm cr}^{(2)}$ the trajectories wander around the period-one fixed points of the map making the growth of I^2 negligible; that is, I^2 becomes almost constant. We call this constant $I_{\rm sat}^2$. Then, for $n > n_{\rm cr}^{(2)}$, the trajectories scape from the influence of the period-one fixed points, and I^2 starts to increase again.

In Fig. 3(a) we also explore the case $I_0 \gg K$ (see open symbols). During the first few iteration steps, since K is small as compared to I_0, I^2 does not increase significantly as a function of n; so, I^2 remains approximately equal to I_0^2 up to a crossover iteration number $n_{\rm cr}^{(0)}$. For $n > n_{\rm cr}^{(0)}$, I^2 follows the same panorama when increasing n as it does in the case of $I_0 \ll K$: it grows up to $n_{\rm cr}^{(1)}$, then it becomes approximately equal to $I_{\rm sat}^2$ up to $n_{\rm cr}^{(2)}$, and finally it grows again.

Then, based on Fig. 3(a), we postulate the following scaling relations:

$$I^2(n, K) \propto n^{\alpha} K^{\beta} \tag{5}$$

for $n < n_{\rm cr}^{(1)}$ and $n > n_{\rm cr}^{(2)}$, with

$$n_{\rm cr}^{(1)}(K) \propto K^{\gamma_1} \tag{6}$$

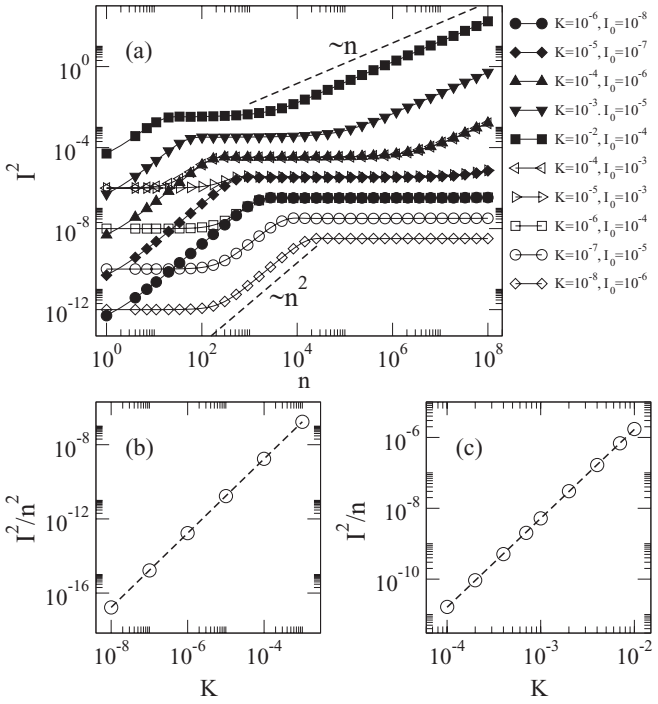

FIG. 3. (a) I^2 as a function of n in the slow diffusion regime ($K \ll 1$). Full symbols (open symbols) correspond to $I_0 \ll K$ ($I_0 \gg K$). Each curve is the average over 1000 trajectories having initial random phases in the interval $0 < \theta_0 < 2\pi$. The dashed lines proportional to n and n^2 are plotted to guide the eye. (b) [(c)] I^2/n^2 [I^2/n] as a function of K for $n < n_{cr}^{(1)}$ [$n > n_{cr}^{(2)}$]. The dashed line equal to $0.17K^2$ [$0.17K^{5/2}$] is the best power-law fit to the data.

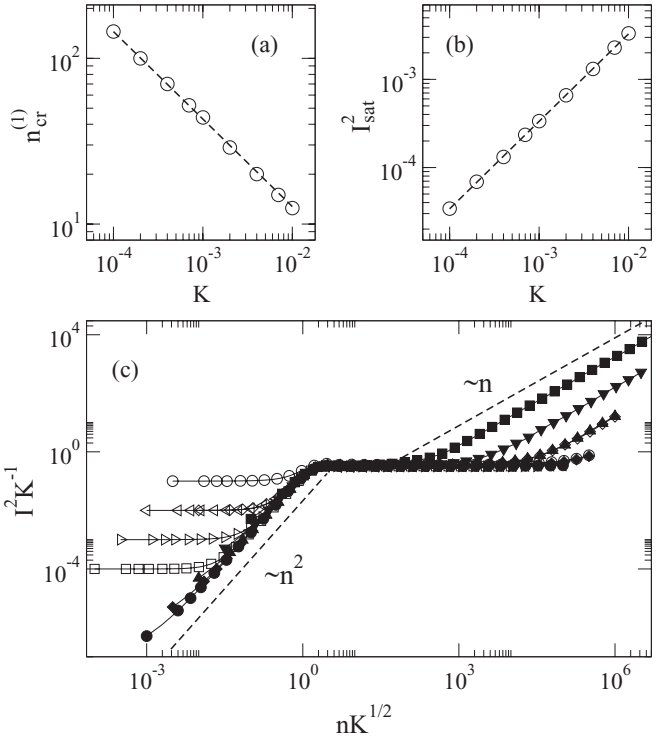

FIG. 4. (a) [(b)] $n_{cr}^{(1)}$ [I_{sat}^2] as a function of K. The dashed line equal to $1.1K^{-1/2}$ [$0.31K$] is the best power-law fit to the data. (c) Scaled curves I^2K^{-1} as a function of $nK^{1/2}$ in the slow diffusion regime ($K \ll 1$). Full symbols (open symbols) correspond to $I_0 \ll K$ ($I_0 \gg K$). Same data as in Fig. 3. The dashed lines show that $I^2 \propto n^2$ for $n < n_{cr}^{(1)}$ while $I^2 \propto n$ for $n > n_{cr}^{(2)}$.

and

$$n_{cr}^{(2)}(K) \propto K^{\gamma_2}; \tag{7}$$

in addition

$$I_{sat}^2(K) \propto K^{\delta}. \tag{8}$$

Also, from Fig. 3(a), we concluded that $n_{cr}^{(0)} = \text{const.} \approx 215$. Below, we present a detailed analysis that allows us to obtain the scaling exponents α, β, $\gamma_{1,2}$, and δ.

By performing power-law fittings to the growth regimes of I^2, we determined that $\alpha \approx 2$ for $n < n_{cr}^{(1)}$ and $\alpha \approx 1$ when $n > n_{cr}^{(2)}$. See dashed lines in Fig. 3(a). Once we know the exponents α, we can extract the exponents β. To this end, in Figs. 3(b) and 3(c), we plot I^2/n^2 for $n < n_{cr}^{(1)}$ and I^2/n for $n > n_{cr}^{(2)}$, respectively, as a function of K. The dashed lines, equal to $0.17K^2$ and $0.17K^{5/2}$, which are the best power-law fits to the data, prove that $\beta \approx 2$ for $n < n_{cr}^{(1)}$ and $\beta \approx 5/2$ when $n > n_{cr}^{(2)}$. In fact, the dependence $I^2 \propto K^{5/2}$ for $n > n_{cr}^{(2)}$ is not surprising since theoretical results for the saw-tooth map [23] as well as numerical computations on the stadium map [9] (both discontinuous maps) show that $I^2 \propto K^{5/2}$ when $K < K_c$ for large n. More precisely, for $K < K_c$ the dynamics of map (2) is diffusive (after the transient time $n_{cr}^{(2)}$) with diffusion rate $D = D_0 K^{5/2}\sqrt{T}$ [8], where $D = \lim_{n\to\infty}\langle I^2(n)\rangle/n$ and the average $\langle\cdots\rangle$ is performed over an ensemble of trajectories with the same initial action I_0 and random initial phases θ_0. $D_0 \approx 0.4$ is the constant that corresponds to the choice of $f(\theta)$ we made here [8].

Then, in Figs. 4(a) and 4(b), we show $n_{cr}^{(1)}$ and I_{sat}^2 as a function of K, respectively. We computed $n_{cr}^{(1)}$ as the intersection of a power-law fitting curve $I^2 \propto n^2$ for $n < n_{cr}^{(1)}$ with the constant curve $I^2 = I_{sat}^2$. The dashed lines in Figs. 4(a) and 4(b) equal to $1.1K^{-1/2}$ and $0.31K$, respectively, lead to $\gamma_1 \approx -1/2$ and $\delta \approx 1$. As a consequence of the scalings above, in Fig. 4(c) we present the scaled curves I^2K^{-1} as a function of $nK^{1/2}$ showing the collapse of I_{sat}^2 and $n_{cr}^{(1)}$.

We want to stress that the scaling of I^2 for the discontinuous map of Eq. (2) in the slow diffusion regime obeys the same scaling laws as CSM in the regime of weak nonlinearity (see [13]), except for the appearance of the second crossover iteration number $n_{cr}^{(2)}$. To study the dependence of $n_{cr}^{(2)}$ on K, in the Fig. 5(inset) we plot $n_{cr}^{(2)}$ vs K. The power-law fitting of the data leads to $\gamma_2 \approx -3/2$ and a proportionality constant $\approx$1.9. Then, in the main panel of Fig. 5 we show that the curves I^2/I_{sat}^2 are properly scaled, for $n > n_{cr}^{(2)}$, when plotting them as a function of $nK^{3/2}$. The behavior $I^2 \propto n$ for $n > n_{cr}^{(2)}$ should be expected in map (2) since here, in contrast to CSM with $K < K_c$, the movement is not bounded by KAM tori, and particles can diffuse along the phase space cylinder without limit.

B. Quasilinear diffusion regime

In Fig. 6(a) we present I^2 as a function of n in the quasilinear diffusion regime ($K \gg 1$) for several combinations of K and I_0.

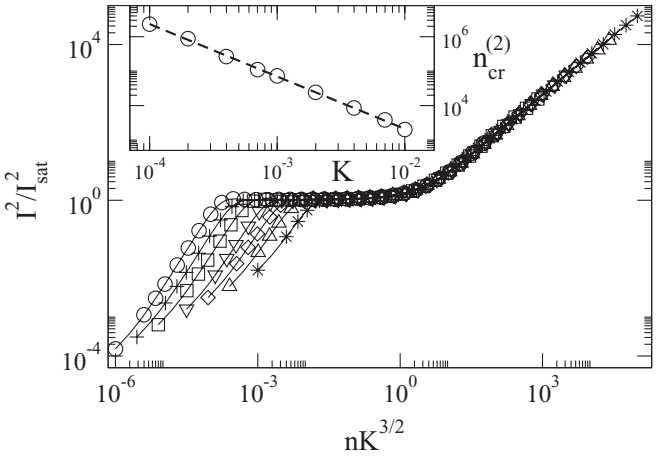

FIG. 5. $I^2/I^2_{\rm sat}$ as a function of $nK^{3/2}$ in the slow diffusion regime ($K \ll 1$). From left to right: $K = 10^{-4}$, 2×10^{-4}, 4×10^{-4}, 10^{-3}, 2×10^{-3}, 4×10^{-3}, and 10^{-2}. $I_0 = K/100$. Inset: $n^{(2)}_{\rm cr}$ as a function of K. The dashed line equal to $1.9K^{-3/2}$ is the best power-law fit to the data.

For $I_0 \ll K$, I^2 grows proportionally to n for all n. See full symbols in Fig. 6(a). For $I_0 \gg K$, I^2 as a function of n is almost constant and approximately equal to I_0^2 up to a crossover iteration number $n_{\rm cr}$. Then, when $n > n_{\rm cr}$, I^2 increases proportionally to n. See open symbols in Fig. 6(a).

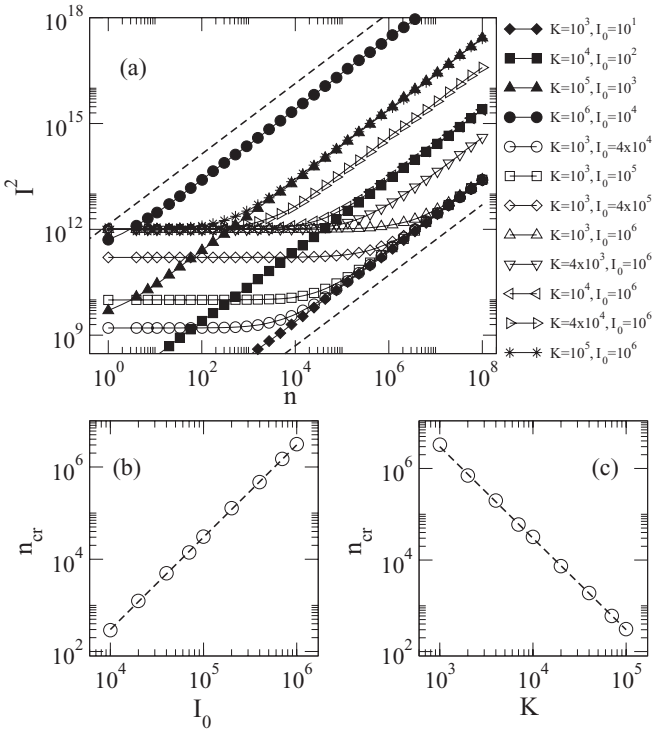

FIG. 6. (a) I^2 as a function of n in the quasilinear diffusion regime ($K \gg 1$). Open symbols (full symbols) correspond to $I_0 \gg K$ ($I_0 \ll K$). Each curve is the average over 1000 trajectories having initial random phases in the interval $0 < \theta_0 < 2\pi$. The dashed lines, plotted to guide the eye, are proportional to n. (b) [(c)] $n_{\rm cr}$ as a function of I_0 [K] for $K = 10^3$ [$I_0 = 10^6$]. The dashed line equal to $3I_0^2$ [$3.1K^{-2}$] is the best power-law fit to the data.

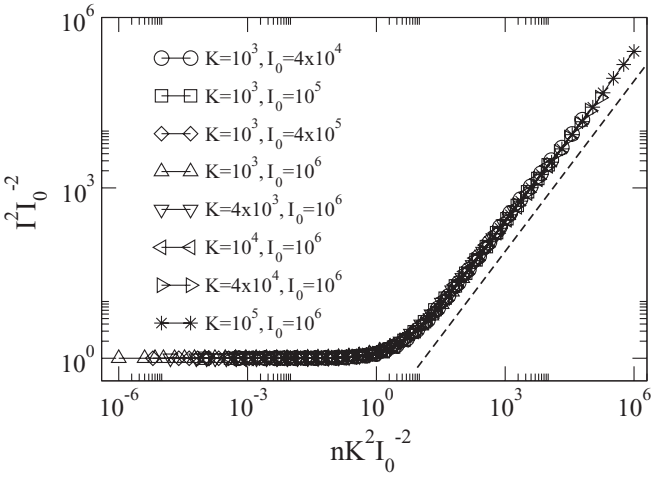

FIG. 7. Scaled curves $I^2 I_0^{-2}$ as a function of $nK^2 I_0^{-2}$ for $I_0 \gg K$. The dashed line shows that $I^2 \propto n$ for $n > n_{\rm cr}$.

This behavior for I^2 is completely equivalent to that for CSM in the strong nonlinearity regime [13]. That is, the scaling given in Eq. (3) is valid for $n > n_{\rm cr}$ with $\alpha \approx 1$ and $\beta \approx 2$. This is consistent with the random phase approximation [3] that predicts, for $K > K_c$, diffusive motion along the I direction with a diffusion rate $D = K^2/2$. Moreover, we observed that the crossover iteration number $n_{\rm cr}$ scales as

$$n_{\rm cr}(K, I_0) \propto K^{\gamma_3} I_0^{\gamma_4}. \tag{9}$$

To get the exponents $\gamma_{3,4}$ in the scaling relation above in Figs. 6(b) and 6(c) we plot (i) $n_{\rm cr}$ as a function of I_0 for fixed K, and (ii) $n_{\rm cr}$ as a function of K for fixed I_0, respectively. Using power-law fittings [see Figs. 6(b) and 6(c)], we found that $n_{\rm cr} \propto K^{-2} I_0^2$ with a proportionality constant $\approx$3. Thus, we concluded that $\gamma_3 \approx -2$ and $\gamma_4 \approx 2$. Finally, from scaling (9), in Fig. 7 we show that all curves $I^2 I_0^{-2}$ as a function of $nK^2 I_0^{-2}$ collapse into a single one.

III. CONCLUSIONS

We have studied the scaling properties of the action variable I for the discontinuous map of Eq. (2). We focus on the slow diffusion ($K < K_c$) and the quasilinear diffusion ($K > K_c$)

TABLE I. Behavior of I^2 in the slow diffusion ($K \ll 1$) and the quasilinear diffusion ($K \gg 1$) regimes. We have found that $I^2_{\rm sat} \approx 0.31K$, $n^{(0)}_{\rm cr} \approx 215$, $n^{(1)}_{\rm cr} \approx 1.1K^{-1/2}$, $n^{(2)}_{\rm cr} \approx 1.9K^{-3/2}$, and $n_{\rm cr} \approx 3I_0^2K^{-2}$.

	$K \ll 1$ $I_0 \ll K$	$K \ll 1$ $I_0 \gg K$	$K \gg 1$ $I_0 \ll K$	$K \gg 1$ $I_0 \gg K$
$I^2 \approx I_0^2$		$n < n^{(0)}_{\rm cr}$		$n < n_{\rm cr}$
$I^2 \propto n^2K^2$	$n < n^{(1)}_{\rm cr}$	$n^{(0)}_{\rm cr} < n < n^{(1)}_{\rm cr}$		
$I^2 \approx I^2_{\rm sat}$	$n^{(1)}_{\rm cr} < n < n^{(2)}_{\rm cr}$	$n^{(1)}_{\rm cr} < n < n^{(2)}_{\rm cr}$		
$I^2 \propto nK^{5/2}$	$n > n^{(2)}_{\rm cr}$	$n > n^{(2)}_{\rm cr}$		
$I^2 \propto nK^2$			$n > n_{\rm cr}$	$n > n_{\rm cr}$

regimes, being $K_c = 1/T$. We found that the scaling of I^2 for map (2) when $K \ll K_c$ and $K \gg K_c$ obey the same scaling laws as CSM in the regimes of weak and strong nonlinearity [13], respectively. Except for that in the slow diffusion regime, due to the absence of KAM tori to bound the motion, $I^2 \propto n$ for large enough n. Also, we conclude that the scaling $I^2 \propto n^\alpha K^\beta$ applies to discontinuous maps with

(i) $\alpha \approx 2$ and $\beta \approx 2$ for $K \ll K_c$ and small n;
(ii) $\alpha \approx 1$ and $\beta \approx 5/2$ for $K \ll K_c$ and large n; and
(iii) $\alpha \approx 1$ and $\beta \approx 2$ for $K \gg K_c$ and large n.

Our results are summarized in Table I.

ACKNOWLEDGMENTS

This work was partially supported by VIEP-BUAP (Grants No. MEBJ-EXC10-I and No. SARA-NAT10-I) and PROMEP (Grants No. 103.5/09/4194 and No. 103.5/10/8442), Mexico.

[1] B. V. Chirikov, Institute of Nuclear Physics, Novosibirsk, Report 267, 1969 (unpublished) [Engl. Transl.: CERN Transl. 71-40 (1971)].
[2] A. J. Lichtenberg and M. A. Lieberman, *Regular and Chaotic Dynamics* (Springer-Verlag, New York, 1992).
[3] B. V. Chirikov, Phys. Rep. **52**, 263 (1979).
[4] J. M. Greene, J. Math. Phys. **20**, 1183 (1979).
[5] R. S. MacKay, Physica D **7**, 283 (1983).
[6] R. S. MacKay, J. D. Meiss, and I. C. Percival, Physica D **13**, 55 (1984).
[7] R. S. MacKay and I. C. Percival, Comm. Math. Phys. **94**, 469 (1985).
[8] F. Borgonovi, Phys. Rev. Lett. **80**, 4653 (1998).
[9] F. Borgonovi, G. Casati, and B. Li, Phys. Rev. Lett. **77**, 4744 (1996).
[10] G. Casati and T. Prosen, Phys. Rev. E **59**, R2516 (1999).
[11] G. Casati and T. Prosen, Phys. Rev. Lett. **85**, 4261 (2000).
[12] T. Prosen and M. Znidaric, Phys. Rev. Lett. **87**, 114101 (2001).
[13] D. G. Ladeira and J. K. L. da Silva, J. Phys. A: Math. Theor. **40**, 11467 (2007).
[14] E. D. Leonel, P. V. E. McClintock, and J. K. L. da Silva, Phys. Rev. Lett. **93**, 014101 (2004).
[15] J. K. L. da Silva, D. G. Ladeira, E. D. Leonel, and P. V. E. Mcclintock, Braz. J. Phys. **36**, 700 (2006).
[16] D. G. Ladeira and J. K. L. da Silva, Phys. Rev. E **73**, 026201 (2006).
[17] E. D. Leonel, J. K. L. da Silva, and S. O. Kamphorst, Physica A **331**, 435 (2004).
[18] E. D. Leonel, Math. Probl. Eng. **2009**, 367921.
[19] E. D. Leonel and P. V. E. Mcclintock, J. Phys. A: Math. Gen. **37**, 8949 (2004); Chaos **15**, 33701 (2005).
[20] E. D. Leonel, Phys. Rev. Lett. **98**, 114102 (2007).
[21] D. G. Ladeira and J. K. L. da Silva, J. Phys. A: Math. Theor. **41**, 365101 (2008).
[22] J. A. de Oliveira, R. A. Bizão, and E. D. Leonel, Phys. Rev. E **81**, 046212 (2010).
[23] I. Dana, N. W. Murray, and I. C. Percival, Phys. Rev. Lett. **62**, 233 (1989).